October 9, 2019
Volume 141
Number 40
pubs.acs.org/JACS

JACS

JOURNAL OF THE AMERICAN CHEMICAL SOCIETY

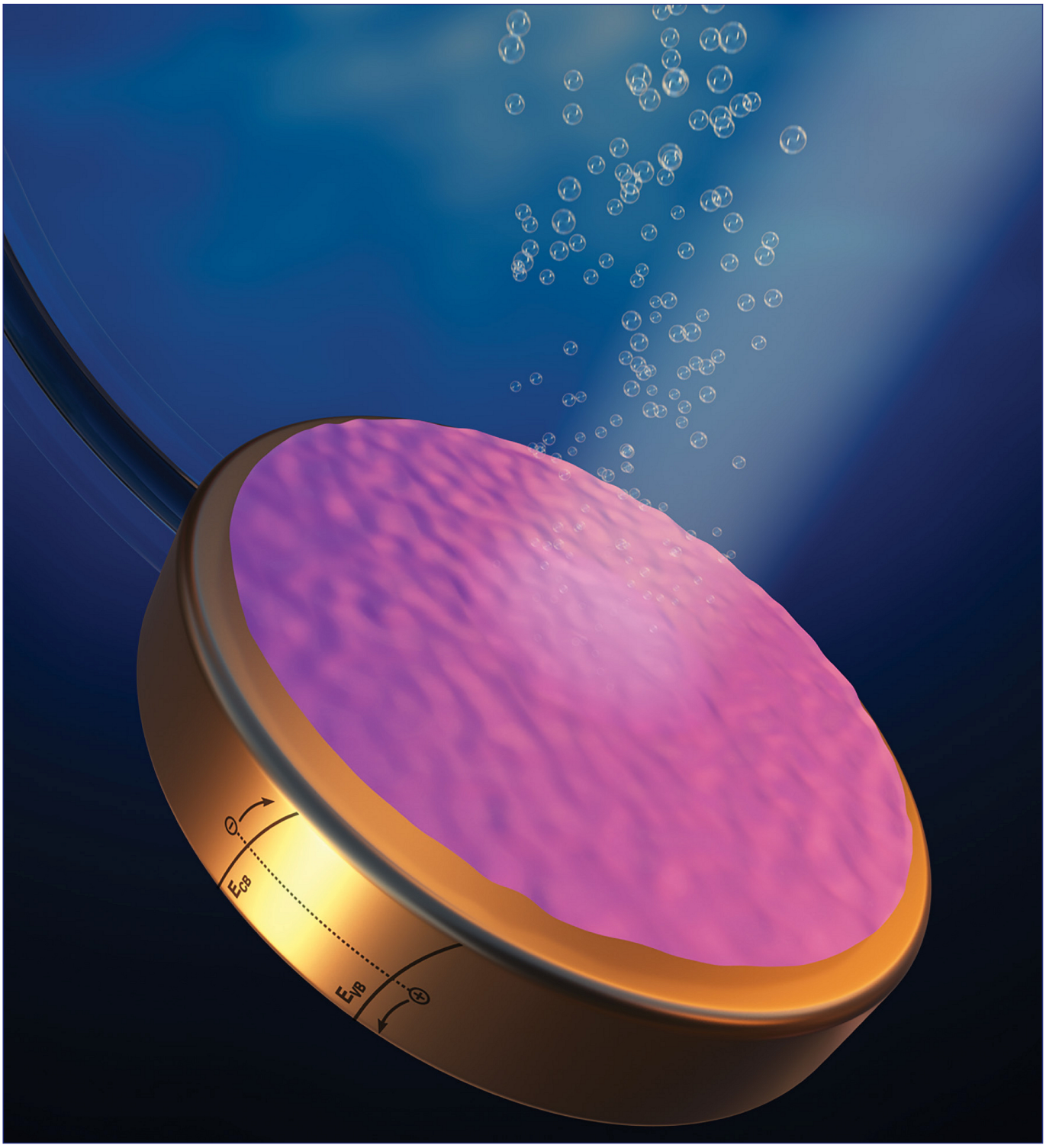

JACS
JOURNAL OF THE AMERICAN CHEMICAL SOCIETY
Article
Cite This: J. Am. Chem. Soc. 2019, 141, 15932−15941
pubs.acs.org/JACS

Interplay between Light Flux, Quantum Efficiency, and Turnover Frequency in Molecular-Modified Photoelectrosynthetic Assemblies

Brian L. Wadsworth, Anna M. Beiler, Diana Khusnutdinova, Edgar A. Reyes Cruz, and Gary F. Moore*

School of Molecular Sciences and the Biodesign Institute Center for Applied Structural Discovery (CASD), Arizona State University, Tempe, Arizona 85287-1604, United States

Supporting Information

ABSTRACT: We report on the interplay between light absorption, charge transfer, and catalytic activity at molecular-catalyst-modified semiconductor liquid junctions. Factors limiting the overall photoelectrosynthetic transformations are presented in terms of distinct regions of experimental polarization curves, where each region is related to the fraction of surface-immobilized catalysts present in their activated form under varying intensities of simulated solar illumination. The kinetics associated with these regions are described using steady-state or pre-equilibrium approximations yielding rate laws similar in form to those applied in studies involving classic enzymatic reactions and Michaelis−Menten-type kinetic analysis. However, in the case of photoelectrosynthetic constructs, both photons and electrons serve as reagents for producing activated catalysts. This work forges a link between kinetic models describing biological assemblies and emerging molecular-based technologies for solar energy conversion, providing a conceptual framework for extracting kinetic benchmarking parameters currently not possible to establish.

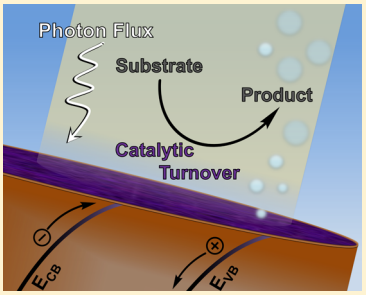

1. INTRODUCTION

Chemical modification of semiconductors with electrocatalysts provides a strategy for developing integrated materials that convert sunlight to fuels and other value-added products.[1,2] In this approach, semiconductors harvest and convert photons into charge carriers moving through a potential and electrocatalysts use the resulting photoelectromotive force to power chemical transformations. In such assemblies, solar energy can drive uphill reactions using photovoltaics coupled to electrolyzers (PV−electrolysis) or photoelectrochemical (PEC) cells. In the latter example, chemical transformations occur at semiconductor|liquid junctions or, in the case of semiconductor surfaces modified with an electrocatalytic layer, electrocatalyst|liquid junctions. PV−electrolysis is at a relatively high technology readiness level, meaning the components are often commercially available.[1] In contrast, PEC devices are at a relatively low technology readiness level but are the focus of research efforts involving several international research teams and individual investigators. Despite their relatively low technology readiness, PEC devices are attractive given their potential to require fewer material components and lower costs associated with installation and operation.[1,3] However, the development of fully integrated architectures remains a major challenge, and advancements are constrained by the availability of effective methods for immobilizing redox catalysts onto semiconductor surfaces as well as an incomplete understanding of fundamental factors limiting their performance.[4,5]

One of the criteria for designing an effective catalyst-modified photoelectrode is to optimize the absorber surface area and catalyst loading with respect to the optical and electrochemical properties of the components.[6,7] In electrocatalysis, a more traditional approach for achieving high activities is to maximize the per geometric area loading of catalysts, typically achieved using high surface area conductive supports. Alternatively, recent studies involving photoactivation of dye-sensitized semiconductors modified with a proxy for a molecular catalyst indicate that relatively low loadings of catalysts can be beneficial for achieving photoinduced charge separation;[8,9] a result likely to spark further studies into identifying design parameters for enhancing performance metrics of complex multicomponent materials. In this vein, advances in high-precision interfacial chemical and material synthesis coupled with surface characterization techniques, theoretical efforts, and modeling are likely to enable an improved understanding of the structure−function relationships governing efficient photon- and electron- driven chemical processes at hybrid material interfaces.[10−21]

Rate laws applying to photoelectrochemical reactions at unmodified semiconductor electrodes have been described[22−28] but have not been extended as widely to molecular-catalyst-modified semiconductors,[6,7,29] and even fewer utilize experimental data to inform the constructed model. Conversely, in the field of homogeneous molecular electrocatalysis, where catalytic reactions occur at an electrode surface and the catalysts are in the same phase as the reactants, the development of electrochemical benchmarking techniques

Received: July 9, 2019
Published: August 28, 2019

DOI: 10.1021/jacs.9b07295
J. Am. Chem. Soc. 2019, 141, 15932−15941

Scheme 1. Gerischer-Type Energy versus Distance Diagram for a p-Type Semiconductor|Liquid Junction under Illumination Showing Photon Absorption, Charge Separation, and Charge Injection Processes;[a] Depiction of an Electrocatalytic System Involving a Conductive Electrode and Homogeneous Molecular Catalyst[b]

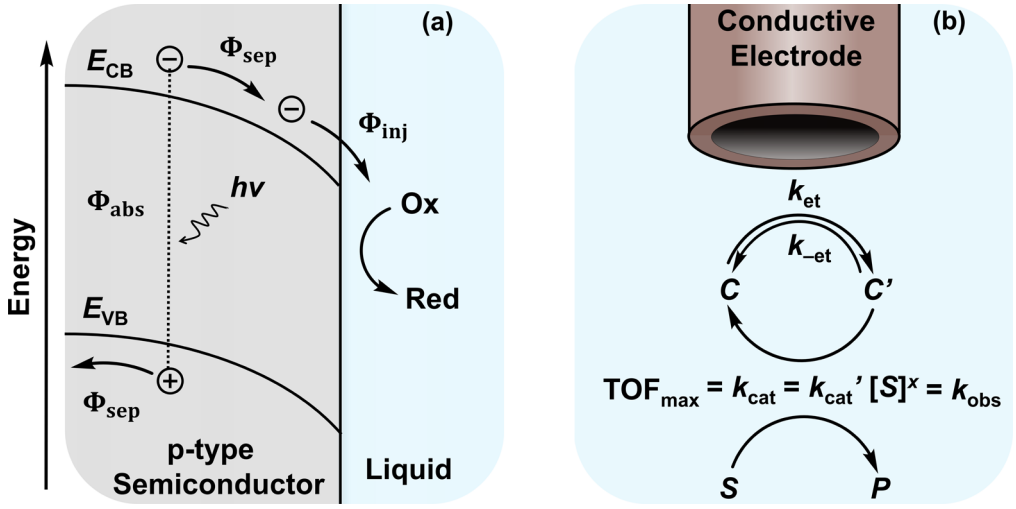

[a]Photons ($h\nu$) are absorbed by the semiconductor, exciting electrons from the valence band (E_{VB}) to the conduction band (E_{CB}). For a p-type semiconductor, minority carrier electrons are directed to the semiconductor surface in contact with solution and majority carrier holes are directed to the back contact. Minority carrier electrons reaching the semiconductor surface can then be injected across the semiconductor|liquid interface to convert oxidized species (Ox) to reduced species (Red). In this scheme, Φ_{abs}, Φ_{sep}, and Φ_{inj} represent the probability of absorption, charge separation, and charge injection, respectively. [b]Charge transfer between a conductive electrode and catalyst (C) produces the activated form of the catalyst (C') that in turn reacts with substrate (S) to form the product (P) and regenerate C. The kinetics are governed by potential-dependent forward and reverse electron transfer rate constants, k_{et} and k_{-et}, respectively, as well as an observed catalytic rate constant, k_{cat}, which is the maximum turnover frequency, TOF_{max}, and is equal to $k_{cat}'[S]^x$, where k_{cat}' is a rate constant for catalysis taking into account the order of the reaction (x) with respect to the concentration of substrate.

has spurred innovations and advancements in catalyst design.[30−34] Such analysis provides information on kinetic parameters, including the maximum turnover frequency (TOF_{max}), which is calculated using the amount of active catalyst present in the reaction-diffusion layer and typically obtained under conditions where the concentration of substrate at the electrode surface is approximately equal to the concentration of the bulk solution (i.e., pure kinetic conditions with no substrate depletion, exhibiting S-shaped wave behavior).[30−32] Under these conditions, the fraction of catalysts at the electrode surface present in their activated form is unity, and the plateau current of the S-shaped voltammogram can be used to calculate an observed rate constant, k_{cat} (sometimes referred to as k_{obs}), which is the TOF_{max}.

For molecular catalysts immobilized at semiconductors, potential-dependent turnover frequencies (TOFs) have been calculated by comparing the surface concentration of the catalytic species to the measured current density after adjusting for nonfaradaic currents. However, in these analyses it is currently not possible to establish a consistent metric and overview of published data based on TOFs since the surface coverage of catalytically active species is unknown or assumed constant and equal to the total or electrochemically active catalyst loading.[4,35] This simplification typically results in an incomplete description of surface kinetics that depend on these coverages, including an accurate determination of k_{cat}, a potential-independent rate constant. Herein, a discussion of kinetic factors governing the rate of photoelectrosynthetic fuel production at molecular-catalyst-modified photocathodes is presented using experimental data. In particular, we address experimental parameters relevant to the rate-limiting step of hydrogen evolution at a cobalt porphyrin-modified gallium phosphide semiconductor in the context of the incident photon flux, quantum efficiency, steady-state concentration of electrons at the semiconductor surface, and related steady-state concentration of immobilized catalysts present in their activated form.

2. RESULTS AND DISCUSSION

2.1. Theory and Elementary Steps of Semiconductor Photoelectrochemistry. The elementary processes of photoelectrochemical reactions were described by Gerischer over 40 years ago,[22,23] and kinetic analyses have been extended and refined in years since.[24−28,36−39] In photoelectrochemical applications, the current density, J, for a photoelectrode under illumination is described according to eq 1, where EQE is the external quantum efficiency, q_p/A is the incident photon flux per geometric area on the surface of the electrode, and e is the electron charge:[40,41]

$$J = \mathrm{EQE} \cdot \frac{q_p}{A} \cdot e \tag{1}$$

EQE, also known as incident photon-to-electron current efficiency, is the ratio of collected charge carriers to the number of incident photons, eq 2, and has been described as one of the most important PEC characteristics.[42,43] It comprises three components:[40]

$$\mathrm{EQE} = \frac{\text{no. of collected carriers, } n}{\text{no. of incident photons, } N} = \Phi_{abs}\Phi_{sep}\Phi_{inj} \tag{2}$$

where Φ_{abs} is the probability of photon absorption, also known as the light-harvesting efficiency (LHE, eq 4), Φ_{sep} is the probability of charge separation within the semiconductor (i.e., splitting of electron—hole (e^-—h^+) pairs), and Φ_{inj} is the

DOI: 10.1021/jacs.9b07295
J. Am. Chem. Soc. 2019, 141, 15932−15941

probability of charge transfer between the semiconductor and a redox-active species. Related to this, the internal quantum efficiency (IQE), eq 3, is the product of the charge separation and charge transfer probabilities:[42]

$$\mathrm{IQE} = \frac{\mathrm{EQE}}{\Phi_{\mathrm{abs}}} = \Phi_{\mathrm{sep}}\Phi_{\mathrm{inj}} \tag{3}$$

As shown in Scheme 1a, photons, hv, are first absorbed by the semiconductor material, generating electron—hole pairs, and the probability of photon absorption, Φ_{abs}, is determined according to eq 4:

$$\Phi_{\mathrm{abs}} = \mathrm{LHE} = 1 - 10^{-A} \tag{4}$$

where A is the absorbance of the photoelectrode.

Once formed, electron—hole pairs can be separated into mobile charge carriers that are directed toward their respective contacts[44] or can recombine via nonradiative and radiative pathways. For a p-type semiconductor, as used in this work, the potential within the semiconductor directs minority carrier electrons to the surface in contact with solution and majority carrier holes to a back contact. The charge separation probability, Φ_{sep}, is defined by eq 5:[40]

$$\Phi_{\mathrm{sep}} = \frac{\text{no. of } e^- \text{ reaching the semiconductor surface}}{\text{no. of } e^- - h^+ \text{ pairs generated}} \tag{5}$$

If the minority carrier diffusion length is short relative to the absorption depth of light in the material, migration of carriers to the surface will suffer. For this reason, spatially identifying recombination events in operando has important implications for the design of improved photoelectrodes, especially in emerging thin-film semiconductors.[45] As described in eq 6, deactivation pathways involving charge recombination processes decrease the probability of charge injection, Φ_{inj}, defined as the ratio of minority carrier electrons injected across the semiconductor surface to the total number of minority carrier electrons reaching the semiconductor surface:[40]

$$\Phi_{\mathrm{inj}} = \frac{\text{no. of } e^- \text{ injected across the semiconductor surface}}{\text{no. of } e^- \text{ reaching the semiconductor surface}} \tag{6}$$

For conducting metallic electrodes, application of an external bias results in a potential drop appearing mostly outside the electrode across an electrical double layer (the Helmholtz layer), and increasing the bias increases the rate constant for electron transfer in accordance with Marcus theory and Butler—Volmer kinetics. In contrast, for an ideal semiconducting electrode[46] the applied bias potential appears mostly inside the semiconductor (the space—charge region), illumination increases the fraction of minority charge carriers reaching the surface, and the rate constant for electron injection across the surface is independent of the applied potential. Thus, dependence of the current density (a rate, not a rate constant) on the applied electrochemical bias is established by changing the degree of band bending within the semiconductor which controls the concentration of charge carriers reaching the surface.

2.2. Theory and Elementary Steps of Homogeneous Molecular Electrocatalysis. Unlike stoichiometric reactions where passage through the highest energy transition state dictates the slow (rate-determining) step, the cyclic nature of catalytic reactions means the overall rate is set by a turnover-limiting step.[47] Further, in electrocatalysis, kinetics associated with heterogeneous electron transfer or catalysis can limit overall reaction rates. As indicated in Scheme 1b, in a catalytic step the activated form of the catalyst, C', reacts with the substrate, S, to form the product, P, with a rate constant k_{cat} and the catalyst, C, is regenerated.

The kinetic analyses used in this report, describing molecular-catalyst-modified photocathodes, are based in part on those initially developed for electrocatalytic reactions comprising a single-electron transfer step followed by a single-chemical step.[48,49] This analysis can and has been extended to describe more complex multistep processes, including hydrogen production, where the catalytic rate constant, k_{cat}, is a global rate constant.[29−32] For electrocatalytic transformations occurring at a conductive surface, the electrode can be polarized at potentials where the rate of interfacial electron transfer is greater than the rate of catalysis; thus, the catalytic step of the overall reaction or the rate of chemical substrate diffusion is considered to be rate limiting. Additionally, the use of relatively high scan rates when recording cyclic voltammograms minimizes depletion of substrate at the electrode surface and thus contributions to the overall kinetics associated with diffusion of chemical substrate (Figure S1).[30] However, in the case of photoelectrosynthetic transformations occurring at a semiconducting surface where the rate constant for electron transfer is potential independent and photons are a reagent, the rate of electron transfer between the semiconductor and the catalyst can be limiting, even at relatively large bias potentials. Guided by these concepts, we present and discuss kinetic models describing a semiconductor modified with molecular catalysts using experimental data.

2.3. Photoelectrosynthesis at Molecular-Catalyst-Modified Semiconductors. To examine the influence of chemical substrate concentration and illumination conditions on photoelectrosynthetic activity, the hydrogen evolution reaction (HER) activity per cobalt center (H_2 s^{-1} Co^{-1}) of cobalt porphyrin—polypyridyl-modified gallium phosphide (CoTTP|PPy|GaP) working electrodes (Figure 1) was measured under varying scan rates, chemical substrate concentrations, and light intensities. In addition, wavelength-resolved EQE measurements were performed to verify the accuracy of the current densities produced during photoelectrochemical experiments involving broadband illumination.[43]

2.3.1. External Quantum Efficiency Analysis. A plot of the wavelength-resolved EQE for a CoTTP|PPy|GaP working electrode polarized at the HER equilibrium potential (i.e., 0 V vs the reversible hydrogen electrode (RHE)) is shown in Figure 2a. The currents are nonzero at wavelengths below 550 nm, consistent with the indirect band gap of GaP. Further, at wavelengths below 450 nm there is a sharp rise in the current due to the direct band gap. The wavelength-resolved EQE reaches a maximum of 59% at 300 nm, and the overall EQE within the absorption range of GaP, considering wavelengths from 280 to 549 nm, is 8.7%.[41,50] Using eq 3, the wavelength-resolved IQE was calculated using the measured EQE (Figure 2a) and quantification of Φ_{abs}, yielding an overall IQE within the absorption range of GaP of 13%[41] (see Figure S2 and Methods).

The quantum efficiency data shown in Figure 2a was also used to obtain an associated wavelength-resolved electron flux spectrum under AM1.5 global tilt solar illumination conditions (Figure 2b). Integration of the resultant electron flux spectrum should in principle equate to the current densities measured

DOI: 10.1021/jacs.9b07295
J. Am. Chem. Soc. 2019, 141, 15932−15941

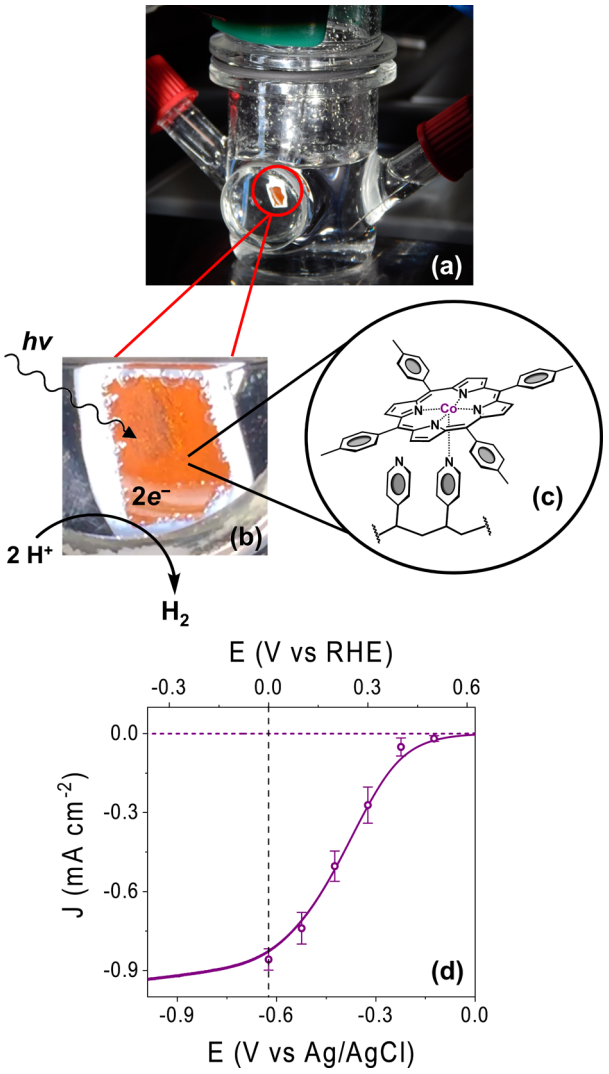

Figure 1. (a) Photograph of a customized photoelectrochemical cell. (b) Close-up image of a CoTTP|PPy|GaP working electrode. (c) Molecular structure of a cobalt porphyrin unit coordinated to a polypyridyl chain. (d) Linear sweep voltammogram with overlaid data from controlled potential electrolysis experiments (circles) recorded using a CoTTP|PPy|GaP working electrode in 0.1 M phosphate buffer (pH 7) under simulated 1-sun illumination (solid) and in the dark (dashed). Vertical dashed line at 0 V vs RHE represents the equilibrium potential of the H^+/H_2 couple.

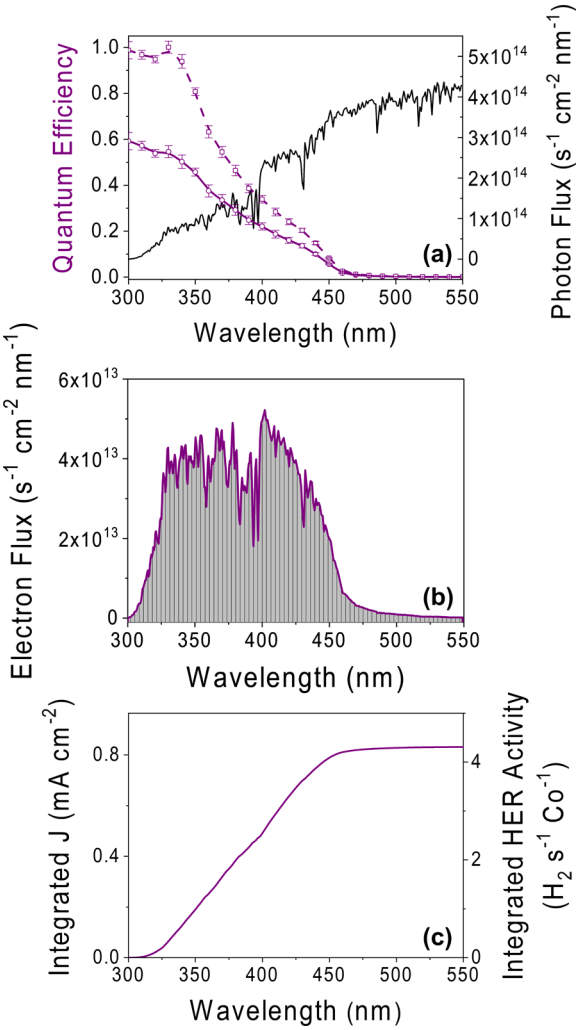

Figure 2. (a) Wavelength-resolved external (circles, solid purple line) and internal (squares, dashed purple line) quantum efficiency plots collected using CoTTP|PPy|GaP working electrodes with a 1 nmol cm^{-2} cobalt loading, polarized at 0 V vs RHE in 0.1 M phosphate buffer (pH 7) as well as the AM1.5 global tilt solar flux spectrum (black solid line). (b) Plot of the wavelength-resolved electron flux calculated using the EQE data shown in panel (a) and considering illumination under AM1.5 global tilt solar flux. (c) Plot produced by integrating the wavelength-resolved electron flux spectrum presented in panel (b); the current density integrated with respect to wavelength is indicted on the left ordinate, and the per cobalt center hydrogen evolution reaction (HER) activity integrated with respect to wavelength is indicated on the right ordinate.

under broadband simulated-solar illumination. However, current densities measured in experiments involving broadband illumination are sometimes overestimated due to factors such as transmittance of epoxy-encased electrodes as well as reflection and transmission losses associated with PEC cell designs.[43] For the constructs reported in this work, integration of the electron flux spectrum under AM1.5 illumination for a CoTTP|PPy|GaP electrode polarized at 0 V vs RHE yields a value of 5.2 ± 0.2 × 10^{15} s^{-1} cm^{-2}, equating to a current density of 0.83 ± 0.03 mA cm^{-2} (Figure 2c). Within the experimental error of these measurements, this value matches the current density of 0.84 ± 0.04 mA cm^{-2} measured under broadband simulated solar conditions (Figure 1d).

2.3.2. Scan Rate and Proton Activity Dependence. A linear sweep voltammogram, recorded using a CoTTP|PPy|GaP working electrode in a neutral pH aqueous solution under 1-sun illumination and a scan rate of 100 mV s^{-1}, is shown in Figure 1d (see Methods). Data obtained from controlled potential electrolysis experiments[51] are overlaid onto this plot, showing that current densities measured under experimental conditions used to collect the linear sweep voltammograms yield values within the experimental error of those measured during controlled potential electrolysis. Further, the current densities produced at 0 V vs RHE in polarization curves recorded under 1-sun illumination in pH-neutral solutions display no measurable scan rate dependence in the 50−2000 mV s^{-1} range (Figures 3a and S3) and show no significant change when adjusting the pH from 4.5 to 10 (Figures 3b and S4). Thus, the HER activity shows a zero-order dependence

DOI: 10.1021/jacs.9b07295
J. Am. Chem. Soc. 2019, 141, 15932−15941

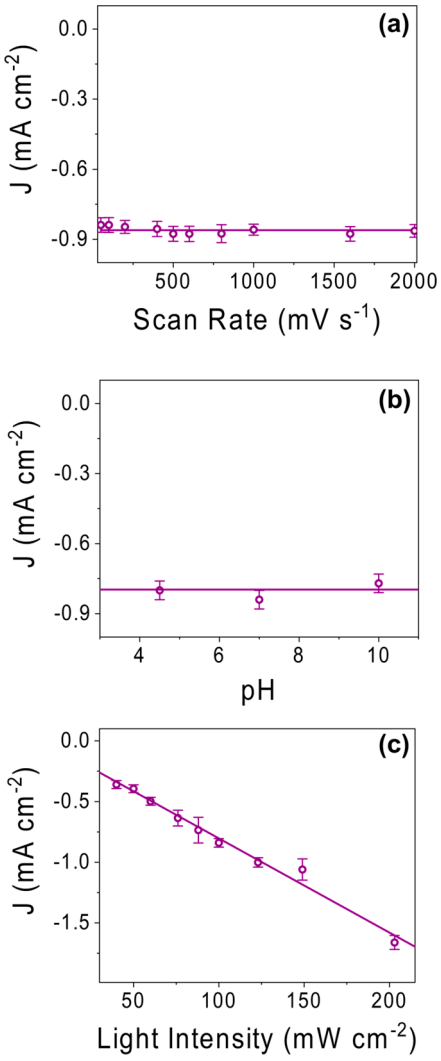

Figure 3. Plots of current densities at 0 V vs RHE recorded using CoTTP|PPy|GaP working electrodes as a function of (a) scan rate, (b) pH, and (c) illumination intensity. All measurements were performed in 0.1 M phosphate buffer (pH 7), except those collected in 0.1 M acetate (pH 4.5) or carbonate−bicarbonate (pH 10) buffers as shown in panel (b).

with respect to proton concentration under these experimental conditions.

2.3.3. Light Intensity Dependence. To assess the dependence of the cobalt porphyrin-modified constructs HER activity with respect to incident photon flux, the HER activity was evaluated under varied illumination intensities (from 0.4 to 2.0 suns) (Figure S5). In these experiments, the current densities recorded at the HER equilibrium potential show a near-linear increase upon increasing the intensity of illumination, indicating the HER activity is first order with respect to photons (Figure 3c).

2.4. Modeling Photoelectrosynthetic Rates at a Molecular-Catalyst-Modified Photocathode. For photoelectrochemical transformations occurring at molecular-catalyst-modified photocathodes, a reaction scheme, including absorption, charge separation, charge injection, and catalysis, is indicated in Figure 4a, where C represents the nonactivated form of the catalyst, e_s^- represents minority carrier electrons at the semiconductor surface, k_{et} is the forward electron transfer rate constant, C' represents the activated form of the catalyst, k_{-et} is the reverse electron transfer rate constant, k_{cat} is an observed rate constant (equal to $k_{cat}'[S]^x$, where k_{cat}' is a rate constant for catalysis taking into account the order of the reaction (x) with respect to the concentration of substrate, $[S]$), and P represents the product. In this reaction scheme the catalytic step is written as a forward, irreversible process due to the irreversible nature of the catalytic reaction.[29,30] Thus, the reverse rate constant, k_{-cat}, is omitted, and the current density response associated with this photoelectrosynthetic scheme is described using eq 7:

$$J = \frac{nF}{FE} k_{cat} \Gamma_{C'} \tag{7}$$

where J is the current density, n is the number of electrons required for the chemical transformation, F is the Faraday constant, FE is the faradaic efficiency, and $\Gamma_{C'}$ is the per geometric area surface density of activated catalysts.

Using CoTTP|PPy|GaP constructs as working electrodes we identified distinct regions in the waveforms of corresponding voltammograms (Figure 4b) that are classified in terms of the concentration of activated catalysts on the electrode surface, which is a function of the photon flux, quantum efficiency, and catalytic turnover. The models developed in this work use analytical expressions where the current densities are expressed in terms of minority carrier currents. This approximation is similar to that used in the Gärtner model[52] and like the Gärtner model, which represents an ideal limiting case, would deviate from experimental results under conditions giving rise to relatively low band bending and high rates of recombination.[37] Models including interfacial minority and majority carrier processes are presented on pp S10 and S11 of the Supporting Information. These models do not change the interpretations presented herein aimed at using concepts developed in studies involving classic enzymatic reactions as well as benchmarking of homogeneous electrocatalysts for extracting an observed catalytic rate constant (k_{cat}) in experiments involving molecular-modified photoelectrosynthetic assemblies.

2.4.1. Nonactive Region. Illuminated CoTTP|PPy|GaP electrodes polarized at potentials positive of the open-circuit voltage produce little to no hydrogen. Additionally, the current density response and related rate of chemical product formation do not significantly change as the applied potential is adjusted within this region. We term this section of the waveform the nonactive region, as the rate of product formation for electrodes operating in this region is near zero and the steady-state concentration of activated catalysts on the electrode surface is negligible.

2.4.2. Potential-Dependent Region. Illuminated CoTTP|PPy|GaP electrodes polarized at potentials negative of the open-circuit voltage produce a current above that measured in the dark. Under these conditions, the degree of band bending within the space charge region, a function of the applied potential, establishes the fraction of minority carrier electrons and majority carrier holes reaching the semiconductor surface and back contact, respectively.[39] Increasing the applied bias potential increases the fraction of minority carrier electrons reaching the semiconductor surface and thus the probability of charge separation and injection to the immobilized catalysts, C, forming activated catalysts, C'. This results in a region of the voltammogram waveform that we term the potential-dependent region, where both the current density, J, and the ratio of C'/C are a function of the applied potential. In this region the

DOI: 10.1021/jacs.9b07295
J. Am. Chem. Soc. 2019, 141, 15932−15941

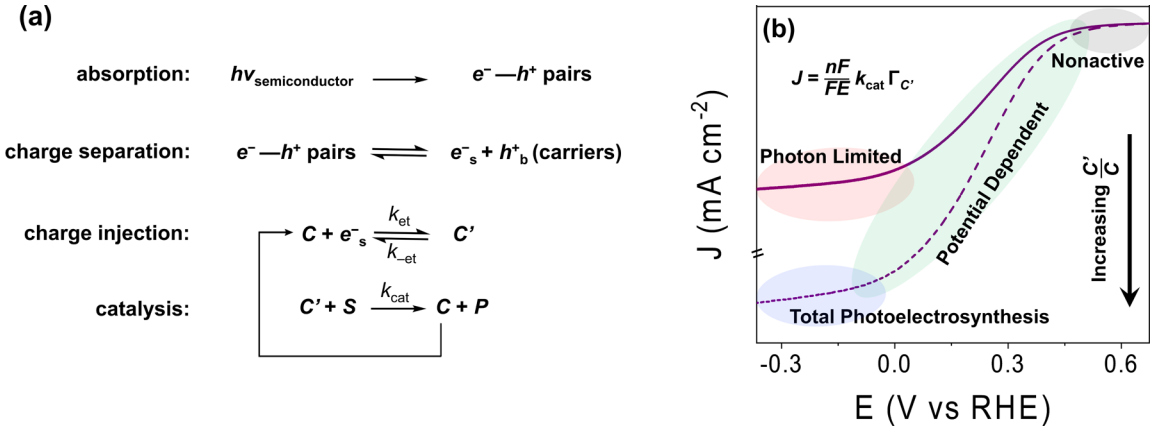

Figure 4. (a) Reaction scheme for photoelectrosynthesis at a molecular-catalyst-modified semiconductor, including (1) absorption of photons ($h\nu$) by the semiconductor to generate electron—hole (e^-—h^+) pairs, (2) charge separation of (e^-—h^+) pairs to form electron minority carriers at the semiconductor surface in contact with solution (e^-_s) and majority carrier holes at the back contact (h^+_b), (3) charge injection of e^-_s from the conduction band to surface-immobilized catalysts (C) forming their activated form (C'), and (4) catalysis, where C' reacts with substrate (S) to form product (P) and regenerate C. (b) Polarization curves at relatively low (solid) or high (dashed) light flux, partitioned into four regions. (1) Nonactive: where the applied potential is positive of the open-circuit potential and the total population of immobilized catalysts are predominantly in their nonactivated form. (2) Potential dependent: where the ratio of C'/C increases as the potential is swept negative. (3) Photon limited: where the steady-state concentration of e^-_s no longer increases as a function of applied potential, resulting in a limiting ratio of C'/C. (4) Total photoelectrosynthesis: where the immobilized catalysts are predominantly present in their activated form.

interfacial electron transfer step is rate limiting and a steady-state approximation,[53,54] where $\frac{d\Gamma_{C'}}{dt} = 0$, is used to describe the current density response (for further details see p S9 in the Supporting Information). Under these conditions, eq 7, describing the current density, J, is re-expressed to yield eq 8:

$$J = \frac{nF}{FE} \cdot \frac{k_{cat}\Gamma_{C_T} n_s}{\frac{k_{-et} + k_{cat}}{k_{et}} + n_s} \tag{8}$$

where Γ_{C_T} and n_s represent the per geometric area surface density of total catalysts and surface electron concentration under steady-state illumination, respectively. At all points in the potential-dependent region the steady-state fraction of immobilized catalysts present in their activated form is less than unity.

Equation 8 is similar in form to the Michaelis–Menten equation used to model enzyme–substrate kinetics when applying a steady-state approximation,[55] where $\frac{k_{-et} + k_{cat}}{k_{et}}$ is analogous to the Michaelis constant, K_m, a term representing the concentration of the chemical substrate required to achieve one-half of the maximum enzymatic activity. Electrochemical forms of the Michaelis–Menten expression have previously been applied to describe the kinetics of redox enzymes (a special category of molecular electrocatalysts) immobilized on conductive electrode surfaces.[29,56] For these constructs, K_m is inherent to a particular redox enzyme and assumed to be independent of the applied potential,[29,56] or the term $\frac{k_{-et} + k_{cat}}{k_{et}}$ becomes quite small since the electrode can be polarized such that $k_{et} \gg k_{-et}$ and $k_{et} \gg k_{cat}$.[29] However, these conditions do not necessarily apply in the case of molecular electrocatalysts immobilized onto semiconductor surfaces where the rate constant for electron transfer is independent of the applied potential and photons as well as electrons are reagents. Accordingly, the constant, $\frac{k_{-et} + k_{cat}}{k_{et}}$, as used in this work, represents the concentration of minority carrier electrons at a semiconductor surface required to activate one-half of the immobilized catalysts. In this context, $\frac{k_{-et} + k_{cat}}{k_{et}}$ is related to the half-wave potential, $E_{cat/2}$,[34] a catalytic benchmark that can be measured under pure kinetic, no substrate-depletion conditions in experiments involving homogeneous molecular electrocatalysts and is the potential required to activate one-half of the catalysts at the electrode surface and thus achieve one-half the maximum activity. Although $E_{cat/2}$ is defined in terms of potential and $\frac{k_{-et} + k_{cat}}{k_{et}}$ is defined in terms of a concentration of minority carrier electrons at a semiconductor surface, we note that the concentration of minority carrier electrons required to activate one-half of the immobilized catalysts is indeed associated with a well-defined potential.

2.4.3. Photon-Limited Region. Upon applying a sufficiently negative bias potential, the current density response of illuminated CoTTP|PPy|GaP electrodes reaches a limiting value that is near potential independent, indicating the steady-state concentration of activated catalysts, $\Gamma_{C'}$, is approximately constant in this region. This response is illustrated in Figures 1d and 4b. As previously mentioned, for the construct reported in this work, increasing the scan rate and proton activity does not alter the value of the limiting current density (Figure 3a and 3b). The limiting behavior and shapes of these waveforms are indeed similar to those associated with S-shaped waves observed in studies involving homogeneous molecular electrocatalysts under pure kinetic, no substrate-depletion conditions.[30−32] However, in the case of these photoelectrosynthetic constructs, the limiting current density can be increased by increasing the incident photon flux. Given the linear relationship between the photon flux and the limiting current densities, we refer to this region of the voltammogram as the photon-limited region. Under these conditions, a steady-state approximation is again applied and eq 8 is used to describe the current density response. We note that kinetic analysis based on the limiting current density achieved in the photon-limited region of a voltammogram would not yield an accurate value of k_{cat} (which is the TOF_{max}) as the steady-state

DOI: 10.1021/jacs.9b07295
J. Am. Chem. Soc. 2019, 141, 15932−15941

concentration of activated catalysts is ill defined and less than unity under these conditions.

2.4.4. Total Photoelectrosynthesis Region. For CoTTP|PPy|GaP constructs operating at the equilibrium potential of the H^+/H_2 couple under 1-sun illumination, experimental results indicate HER activity is not limited by a catalytic step (energy storage) where all of the catalyst species are in their activated form but instead is limited by kinetics associated with light capture and conversion. This implies that a region where the current density is potential independent and no longer limited by photon flux (i.e., where the steady-state concentration of the activated catalyst is unity) may exist. In this region, termed the total photoelectrosynthesis region in Figure 4b, the catalysis step indicated in Figure 4a would be rate limiting. Under such conditions, a pre-equilibrium approximation[53] could be used to model the limiting current density response. Using this approximation, eq 7, describing the current density, J, is re-expressed to yield eq 9:

$$J = \frac{nF}{FE} \cdot \frac{k_{cat}\Gamma_{C_T} n_s}{K^{-1} + n_s} \tag{9}$$

where K^{-1} is an equilibrium constant equal to the ratio of the forward and reverse rate constants for electron transfer from the semiconductor, $\frac{k_{-et}}{k_{et}}$ (for further details see p S9 in the Supporting Information).

Equation 9 is similar in form to rate laws associated with Michaelis–Menten enzyme–substrate kinetics when applying a pre-equilibrium approximation,[55] where K^{-1} is analogous to the ligand–receptor affinity constant, K_d. If product formation is occurring only at activated molecular catalyst sites, the saturating current density provides an opportunity to extrapolate a value for k_{cat},[57] but to our knowledge such measurements have yet to be reported using a molecular-catalyst-modified semiconductor. Although distinct regions of the voltammograms in Figure 4b are indicated for simplicity, in practice a transition from the photon-limited region to the total photoelectrosynthesis region would be continuous and likely include a region where both steady-state and pre-equilibrium approximations can be applied.[58]

2.5. Photon and Electron Flux with Respect to Catalytic Loading and Turnover. Nonimmobilized molecular electrocatalysts have been reported with values of TOF_{max} ranging from 0.1 to 2 000 000 s^{-1}.[29,30,59] Given an active catalyst loading of 1 nmol cm^{-2}, a loading representative of the total cobalt loading for the constructs reported in this work, the electron flux required to produce hydrogen at rates from 0.1 to 2 000 000 s^{-1} $site^{-1}$ would be from 1.2×10^{13} to 2.4×10^{21} s^{-1} cm^{-2} (from 2×10^{-6} to 400 A cm^{-2}). For comparison, the total photon flux (integrating from 280 to 4000 nm) under AM1.5 global tilt solar illumination is 4.3×10^{17} s^{-1} cm^{-2}. If a photoelectrode or device utilized this photon flux with unity EQE across all wavelengths (280 to 4000 nm) it would operate at a current density of 0.069 A cm^{-2}.

Given the illumination conditions used in this report (ranging from 0.4 to 2.0 suns), a GaP semiconductor electrode with a 2.26 eV indirect band gap would be capable of generating current densities ranging from 3.8×10^{-3} to 19.2×10^{-3} A cm^{-2} if the electrode operated with 100% EQE at all wavelengths below the GaP indirect band gap. At a 1 nmol cm^{-2} loading of active catalysts, this range of current densities would require electron fluxes to each active site ranging from 40 to 200 s^{-1} $site^{-1}$ when operating with unity faradaic efficiency, yielding an HER activity of 20–100 H_2 s^{-1} $site^{-1}$ (Figure S6). The actual current densities measured using CoTTP|PPy|GaP working electrodes described in this report (polarized at the HER equilibrium potential and measured under 0.4–2.0 suns illumination) range from 0.36×10^{-3} to 1.70×10^{-3} A cm^{-2}. This equates to a per cobalt center electron flux of 4–20 s^{-1} Co $site^{-1}$ and a per cobalt center HER activity of 2–10 H_2 s^{-1} Co $site^{-1}$. Higher per metal site HER activities have previously been reported for cobalt porphyrin-modified semiconductors;[19,20] however, these constructs were prepared using GaP wafers with intrinsic differences in the semiconductor characteristics (including the resistivity, mobility, and carrier concentration) as well as different per geometric area catalyst loadings. These results indicate that a more than doubling of the catalysts loading, from 0.4 to 1 nmol cm^{-2}, does not result in higher HER activity, illustrating that a higher catalyst loading does not always correlate with increased photoelectrosynthetic activity as we propose is the case for photoelectrodes operating under photon-limiting conditions.

3. CONCLUSION

Kinetic models constructed from experimental results are used to rationalize rates of photoelectrosynthetic fuel production at molecular-catalyst-modified photoelectrode surfaces. The analytical expressions developed in this work have parallels with rate laws describing the catalytic behavior of enzymes in Michaelis–Menten-type kinetic analyses and molecular electrocatalysts, forging a link between kinetic models used to describe heterogeneous, homogeneous, and biocatalytic systems. However, in photoelectrosynthetic constructs, both photons and electrons serve as substrates. Although the studies described in this report focus on hydrogen evolution using metalloporphyrin-modified gallium phosphide semiconductors, the analysis and discussions related to the interplay between illumination conditions, quantum efficiency, and fuel production activity are likely applicable to a broader range of photoelectrosynthetic assemblies, providing a conceptual model for studying and better understanding fundamental factors limiting their performance.

4. METHODS

4.1. Sample Preparation. The cobalt porphyrin–polypyridyl-modified GaP photoelectrodes (CoTTP|PPy|GaP) used in this report were prepared following a previously reported method[20] (see Supporting Information for further details).

4.2. Photoelectrochemical Measurements. All electrochemical measurements were performed using a Biologic potentiostat equipped with a platinum coil counter electrode, a Ag/AgCl, NaCl (3 M) reference electrode (0.21 V vs NHE), and functionalized GaP working electrodes in a modified cell containing a quartz window. Linear sweep voltammograms were recorded in the dark and under 100 mW cm^{-2} illumination using a 100 W Oriel Solar Simulator equipped with an AM1.5 filter. The supporting electrolytes were 0.1 M acetate (pH 4.5), phosphate (pH 7), and carbonate–bicarbonate (pH 10) buffers. Linear sweep voltammograms were recorded at sweep rates of 50–2000 mV s^{-1} under a continuous flow of 5% hydrogen in nitrogen. Controlled potential electrolysis experiments were performed with the working electrode polarized at a selected potential for 1 min and the reported current density is the average value over that time interval.

4.3. External Quantum Efficiency Measurements. The external quantum efficiency was measured under a bias of 0 V vs RHE (where E vs RHE = E vs NHE + 0.05916 V × pH = E vs Ag/

DOI: 10.1021/jacs.9b07295
J. Am. Chem. Soc. 2019, 141, 15932–15941

AgCl + 0.05916 V × pH + 0.21 V) in the wavelength range of 300−600 nm. The experimental setup consisted of a Biologic potentiostat and the QEPVSI-b Quantum Efficiency Measurement System from Newport Corporation, including a reference detector with NIST-traceable responsivity data, a 300 W Oriel xenon lamp, and an Oriel Cornerstone 260 monochromator. Data were collected at 10 nm intervals, with a 300 ms pause between steps. The current was collected at 2 points/s, and the data collected at each wavelength were averaged. The dark current before and after the experiment was subtracted from the current produced under illumination. The photon flux at a particular wavelength (q_p) was determined using the voltage response of the reference detector in accordance with eq 10:

$$q_p = \frac{(V)}{(CR)(SR)(Gain)E(\lambda)} \tag{10}$$

where V is the detector voltage, CR is the correction multiplier of the ac measurement, SR is the spectral responsivity of the reference detector, $Gain$ is the gain set for the detector, and $E(\lambda)$ is the energy of a photon at a given wavelength.

4.4. Internal Quantum Efficiency Measurements. The internal quantum efficiency was calculated by dividing the measured external quantum efficiency values by the light-harvesting efficiency at each wavelength of interest. The light-harvesting efficiency was determined by calculating the absorbance and absorption coefficient of a CoTTP|PPy|GaP sample using eqs 11 and 12:[60,61]

$$A = \frac{\alpha \cdot L}{\ln 10} \tag{11}$$

$$\alpha = -\ln\left[\frac{(\%T + \%R)}{100}\right]/L \tag{12}$$

where α is the wavelength-dependent absorption coefficient, L is the path length or thickness of the GaP wafer (400 μm), $\%T$ represents the percent transmittance collected at normal incidence, and $\%R$ represents the sum of the specular percent reflectance, collected at an incident angle of 5° to the normal of the surface, and diffuse percent reflectance. Under the same cell and polarization conditions used to collect the external quantum efficiency, the internal quantum efficiency calculated within the photoactive region of GaP reaches a maximum of 100% at 330 nm.

■ ASSOCIATED CONTENT

Supporting Information

The Supporting Information is available free of charge on the ACS Publications website at DOI: 10.1021/jacs.9b07295.

Additional supporting details for experimental methods and equations, as well as additional optical spectra and electrochemical data (PDF)

■ AUTHOR INFORMATION

Corresponding Author

*gary.f.moore@asu.edu

ORCID

Brian L. Wadsworth: 0000-0002-0274-9993

Gary F. Moore: 0000-0003-3369-9308

Author Contributions

The manuscript was written through contributions of all authors. All authors have given approval to the final version of the manuscript

Notes

The authors declare no competing financial interest.

■ ACKNOWLEDGMENTS

This research was supported by the National Science Foundation under Early Career Award 1653982 and the College of Liberal Arts and Sciences at Arizona State University and Biodesign Institute Center for Applied Structural Discovery (CASD). B.L.W. and A.M.B. were supported by an IGERT-SUN fellowship funded by the National Science Foundation (1144616) and the Phoenix Chapter of the ARCS Foundation. A.M.B received additional support from the P.E.O Scholar Award.

■ REFERENCES

(1) Ardo, S.; Fernandez Rivas, D. F.; Modestino, M. A.; Schulze Greiving, V. S.; Abdi, F. F.; Alarcon Llado, E. A.; Artero, V.; Ayers, K.; Battaglia, C.; Becker, J.-P.; Bederak, D.; Berger, A.; Buda, F.; Chinello, E.; Dam, B.; Di Palma, V.; Edvinsson, T.; Fujii, K.; Gardeniers, H.; Geerlings, H.; Hashemi, S. M. H.; Haussener, S.; Houle, F.; Huskens, J.; James, B. D.; Konrad, K.; Kudo, A.; Kunturu, P. P.; Lohse, D.; Mei, B.; Miller, E. L.; Moore, G. F.; Muller, J.; Orchard, K. L.; Rosser, T. E.; Saadi, F. H.; Schüttauf, J.-W.; Seger, B.; Sheehan, S. W.; Smith, W. A.; Spurgeon, J.; Tang, M. H.; van de Krol, R.; Vesborg, P. C. K.; Westerik, P. Pathways to Electrochemical Solar-Hydrogen Technologies. *Energy Environ. Sci.* **2018**, *11*, 2768−2783.

(2) Faunce, T. A.; Lubitz, W.; Rutherford, A. W.; MacFarlane, D.; Moore, G. F.; Yang, P.; Nocera, D. G.; Moore, T. A.; Gregory, D. H.; Fukuzumi, S.; Yoon, K. B.; Armstrong, F. A.; Wasielewski, M. R.; Styring, S. Energy and Environment Policy Case for a Global Project on Artificial Photosynthesis. *Energy Environ. Sci.* **2013**, *6*, 695−698.

(3) Shaner, M. R.; Atwater, H. A.; Lewis, N. S.; McFarland, E. W. A Comparative Technoeconomic Analysis of Renewable Hydrogen Production Using Solar Energy. *Energy Environ. Sci.* **2016**, *9*, 2354−2371.

(4) Kibsgaard, J.; Chorkendorff, I. Considerations for the Scaling-Up of Water Splitting Catalysts. *Nat. Energy* **2019**, *4*, 430−433.

(5) McKone, J. R.; Marinescu, S. C.; Brunschwig, B. S.; Winkler, J. R.; Gray, H. B. Earth-Abundant Hydrogen Evolution Electrocatalysts. *Chem. Sci.* **2014**, *5*, 865−878.

(6) Lin, F.; Boettcher, S. W. Adaptive Semiconductor/Electrocatalyst Junctions in Water-Splitting Photoanodes. *Nat. Mater.* **2014**, *13*, 81−86.

(7) Mills, T. J.; Lin, F.; Boettcher, S. W. Theory and Simulations of Electrocatalyst-Coated Semiconductor Electrodes for Solar Water Splitting. *Phys. Rev. Lett.* **2014**, *112*, 1−5.

(8) Chen, H. Y.; Ardo, S. Direct Observation of Sequential Oxidations of a Titania-Bound Molecular Proxy Catalyst Generated Through Illumination of Molecular Sensitizers. *Nat. Chem.* **2018**, *10*, 17−23.

(9) Beiler, A. M.; Moore, G. F. Multi-Electron Transfer Photochemistry: Caught in the Act. *Nat. Chem.* **2018**, *10*, 3−4.

(10) Ye, R.; Zhao, J.; Wickemeyer, B. B.; Toste, F. D.; Somorjai, G. A. Foundations and Strategies of the Construction of Hybrid Catalysts for Optimized Performances. *Nat. Catal.* **2018**, *1*, 318−325.

(11) Hou, Y.; Abrams, B. L.; Vesborg, P. C. K.; Björketun, M. E.; Herbst, K.; Bech, L.; Setti, A. M.; Damsgaard, C. D.; Pedersen, T.; Hansen, O.; Rossmeisl, J.; Dahl, S.; Nørskov, J. K.; Chorkendorff, I. Bioinspired Molecular Co-Catalysts Bonded to a Silicon Photocathode for Solar Hydrogen Evolution. *Nat. Mater.* **2011**, *10*, 434−438.

(12) Queyriaux, N.; Kaeffer, N.; Morozan, A.; Chavarot-Kerlidou, M.; Artero, V. Molecular Cathode and Photocathode Materials for Hydrogen Evolution in Photoelectrochemical Devices. *J. Photochem. Photobiol., C* **2015**, *25*, 90−105.

(13) Bullock, R. M.; Das, A. K.; Appel, A. M. Surface Immobilization of Molecular Electrocatalysts for Energy Conversion. *Chem. - Eur. J.* **2017**, *23*, 7626−7641.

DOI: 10.1021/jacs.9b07295
J. Am. Chem. Soc. 2019, 141, 15932−15941

(14) Wadsworth, B. L.; Khusnutdinova, D.; Moore, G. F. Polymeric Coatings for Applications in Electrocatalytic and Photoelectrosynthetic Fuel Production. *J. Mater. Chem. A* **2018**, *6*, 21654−21665.
(15) Downes, C. A.; Marinescu, S. C. Efficient Electrochemical and Photoelectrochemical H_2 Production from Water by a Cobalt Dithiolene One-Dimensional Metal−Organic Surface. *J. Am. Chem. Soc.* **2015**, *137*, 13740−13743.
(16) Leung, J. J.; Warnan, J.; Ly, K. H.; Heidary, N.; Nam, D. H.; Kuehnel, M. F.; Reisner, E. Solar-Driven Reduction of Aqueous CO_2 with a Cobalt Bis (Terpyridine)-Based Photocathode. *Nat. Catal.* **2019**, *2*, 354−365.
(17) Gu, J.; Yan, Y.; Young, J. L.; Steirer, K. X.; Neale, N. R.; Turner, J. A. Water Reduction by a p-$GaInP_2$ Photoelectrode Stabilized by an Amorphous TiO_2 Coating and a Molecular Cobalt Catalyst. *Nat. Mater.* **2016**, *15*, 456−460.
(18) Krawicz, A.; Yang, J.; Anzenberg, E.; Yano, J.; Sharp, I. D.; Moore, G. F. Photofunctional Construct that Interfaces Molecular Cobalt-Based Catalysts for H_2 Production to a Visible-Light-Absorbing Semiconductor. *J. Am. Chem. Soc.* **2013**, *135*, 11861−11868.
(19) Khusnutdinova, D.; Beiler, A. M.; Wadsworth, B. L.; Jacob, S. I.; Moore, G. F. Metalloporphyrin-Modified Semiconductors for Solar Fuel Production. *Chem. Sci.* **2017**, *8*, 253−259.
(20) Beiler, A. M.; Khusnutdinova, D.; Wadsworth, B. L.; Moore, G. F. Cobalt Porphyrin−Polypyridyl Surface Coatings for Photoelectrosynthetic Hydrogen Production. *Inorg. Chem.* **2017**, *56*, 12178−12185.
(21) Osterloh, F. E. Photocatalysis Versus Photosynthesis: A Sensitivity Analysis of Devices for Solar Energy Conversion and Chemical Transformations. *ACS Energy Lett.* **2017**, *2*, 445−453.
(22) Gerischer, H. Charge Transfer Processes at Semiconductor-Electrolyte Interfaces in Connection with Problems of Catalysis. *Surf. Sci.* **1969**, *18*, 97−122.
(23) Gerischer, H. Electrochemical Photo and Solar Cells Principles and Some Experiments. *J. Electroanal. Chem. Interfacial Electrochem.* **1975**, *58*, 263−274.
(24) Gerischer, H. The Role of Semiconductor Structure and Surface Properties in Photoelectrochemical Processes. *J. Electroanal. Chem. Interfacial Electrochem.* **1983**, *150*, 553−569.
(25) Gerischer, H. Electron-Transfer Kinetics of Redox Reactions at the Semiconductor/Electrolyte Contact. A New Approach. *J. Phys. Chem.* **1991**, *95*, 1356−1359.
(26) Lewis, N. S. An Analysis of Charge Transfer Rate Constants for Semiconductor/Liquid Interfaces. *Annu. Rev. Phys. Chem.* **1991**, *42*, 543−580.
(27) Nozik, A. J. Photoelectrochemistry: Applications to Solar Energy Conversion. *Annu. Rev. Phys. Chem.* **1978**, *29*, 189−222.
(28) Le Formal, F.; Pastor, E.; Tilley, S. D.; Mesa, C. A.; Pendlebury, S. R.; Grätzel, M.; Durrant, J. R. Rate Law Analysis of Water Oxidation on a Hematite Surface. *J. Am. Chem. Soc.* **2015**, *137*, 6629−6637.
(29) Sathrum, A. J.; Kubiak, C. P. Kinetics and Limiting Current Densities of Homogeneous and Heterogeneous Electrocatalysts. *J. Phys. Chem. Lett.* **2011**, *2*, 2372−2379.
(30) Artero, V.; Savéant, J.-M. Toward the Rational Benchmarking of Homogeneous H_2-Evolving Catalysts. *Energy Environ. Sci.* **2014**, *7*, 3808−3814.
(31) Costentin, C.; Savéant, J.-M. Towards an Intelligent Design of Molecular Electrocatalysts. *Nat. Rev. Chem.* **2017**, *1*, 0087.
(32) Lee, K. J.; Elgrishi, N.; Kandemir, B.; Dempsey, J. L. Electrochemical and Spectroscopic Methods for Evaluating Molecular Electrocatalysts. *Nat. Rev. Chem.* **2017**, *1*, 0039.
(33) Bligaard, T.; Bullock, R. M.; Campbell, C. T.; Chen, J. G.; Gates, B. C.; Gorte, R. J.; Jones, C. W.; Jones, W. D.; Kitchin, J. R.; Scott, S. L. Toward Benchmarking in Catalysis Science: Best Practices, Challenges, and Opportunities. *ACS Catal.* **2016**, *6*, 2590−2602.
(34) Appel, A. M.; Helm, M. L. Determining the Overpotential for a Molecular Electrocatalyst. *ACS Catal.* **2014**, *4*, 630−633.
(35) In practice, the steady-state concentration of catalysts in their activated form can vary as a function of the applied bias potential.
(36) Nozik, A. J.; Memming, R. Physical Chemistry of Semiconductor-Liquid Interfaces. *J. Phys. Chem.* **1996**, *100*, 13061−13078.
(37) Peter, L. M. Dynamic Aspects of Semiconductor Photoelectrochemistry. *Chem. Rev.* **1990**, *90*, 753−769.
(38) Bard, A. J.; Bocarsly, A. B.; Fan, F. F.; Walton, E. G.; Wrighton, M. S. The Concept of Fermi Level Pinning at Semiconductor/Liquid Junctions. Consequences for Energy Conversion Efficiency and Selection of Useful Solution Redox Couples in Solar Devices. *J. Am. Chem. Soc.* **1980**, *102*, 3671−3677.
(39) Peter, L. M. Energetics and Kinetics of Light-Driven Oxygen Evolution at Semiconductor Electrodes: The Example of Hematite. *J. Solid State Electrochem.* **2013**, *17*, 315−326.
(40) Dotan, H.; Sivula, K.; Grätzel, M.; Rothschild, A.; Warren, S. C. Probing the Photoelectrochemical Properties of Hematite (α-Fe_2O_3) Electrodes Using Hydrogen Peroxide as a Hole Scavenger. *Energy Environ. Sci.* **2011**, *4*, 958−964.
(41) EQE and IQE are defined at a specified wavelength. However, they can also be described as a single parameter integrated over a specified spectral range.
(42) Chen, Z.; Jaramillo, T. F.; Deutsch, T. G.; Kleiman-Shwarsctein, A.; Forman, A. J.; Gaillard, N.; Garland, R.; Takanabe, K.; Heske, C.; Sunkara, M.; McFarland, E. W. Accelerating Materials Development for Photoelectrochemical Hydrogen Production: Standards for Methods, Definitions, and Reporting Protocols. *J. Mater. Res.* **2010**, *25*, 3−16.
(43) Döscher, H.; Young, J. L.; Geisz, J. F.; Turner, J. A.; Deutsch, T. G. Solar-to-Hydrogen Efficiency: Shining Light on Photoelectrochemical Device Performance. *Energy Environ. Sci.* **2016**, *9*, 74−80.
(44) Würfel, U.; Cuevas, A.; Würfel, P. Charge Carrier Separation in Solar Cells. *IEEE J. Photovolt.* **2015**, *5*, 461−469.
(45) Segev, G.; Jiang, C. M.; Cooper, J. K.; Eichhorn, J.; Toma, F. M.; Sharp, I. D. Quantification of the Loss Mechanisms in Emerging Water Splitting Photoanodes Through Empirical Extraction of the Spatial Charge Collection Efficiency. *Energy Environ. Sci.* **2018**, *11*, 904−913.
(46) For a nonideal semiconductor, the presence of surface states can introduce additional energy levels which pin the band edges relative to the Fermi level, affecting the maximum obtainable photovoltage. See ref 38.
(47) Crabtree, R. H. *The Organometallic Chemistry of the Transition Metals*, 4th ed.; John Wiley & Sons: Hoboken, NJ, 2014.
(48) Delahay, P.; Stiehl, G. L. Theory of Catalytic Polargraphic Currents. *J. Am. Chem. Soc.* **1952**, *74*, 3500−3505.
(49) Savéant, J. M.; Vianello, E. Potential-Sweep Chronoamperometry. Kinetic Currents for First-Order Chemical Reaction Parallel to Electron-Transfer Process (Catalytic Currents). *Electrochim. Acta* **1965**, *10*, 905−920.
(50) The overall external quantum efficiency for CoTTP|PPy|GaP electrodes polarized at 0 V vs RHE, considering the spectral range from 280 to 4000 nm, is 1.2%.
(51) The CoTTP|PPy|GaP photocathode was polarized at the indicated potential for 1 min, and the current density was reported as the average value. The measured current densities decreased by no more than 6% over the 1 min polarization period for each potential selected.
(52) Gärtner, W. W. Depletion-Layer Photoeffects in Semiconductors. *Phys. Rev.* **1959**, *116*, 84−87.
(53) Pyun, C. W. Steady-State and Equilibrium Approximations in Chemical Kinetics. *J. Chem. Educ.* **1971**, *48*, 194−196.
(54) Briggs, G. E.; Haldane, J. B. S. A Note on the Kinetics of Enzyme Action. *Biochem. J.* **1925**, *19*, 338−339.
(55) Johnson, K. A.; Goody, R. S. The Original Michaelis Constant: Translation of the 1913 Michaelis−Menten Paper. *Biochemistry* **2011**, *50*, 8264−8269.
(56) Sucheta, A.; Cammack, R.; Weiner, J.; Armstrong, F. A. Reversible Electrochemistry of Fumarate Reductase Immobilized on an Electrode Surface. Direct Voltammetric Observations of Redox

DOI: 10.1021/jacs.9b07295
J. Am. Chem. Soc. 2019, 141, 15932−15941

Centers and their Participation in Rapid Catalytic Electron Transport. *Biochemistry* **1993**, *32*, 5455−5465.
(57) The model presented herein does not address background activity due to surface sites that could introduce parallel kinetic pathways but in principle could be adapted to include such. As presented in the current model, the value of k_{cat} would represent an upper limit if competing kinetic pathways contribute to product formation.
(58) By applying simplifying assumptions, the current density equations derived using the steady-state or pre-equilibrium approximation reduce to a common result, termed the equilibrium-steady-state solution. See ref 53.
(59) Khusnutdinova, D.; Wadsworth, B. L.; Flores, M.; Beiler, A. M.; Reyes Cruz, E. A.; Zenkov, Y.; Moore, G. F. Electrocatalytic Properties of Binuclear Cu(II) Fused Porphyrins for Hydrogen Evolution. *ACS Catal.* **2018**, *8*, 9888−9898.
(60) Sze, S. M.; Ng, K. K. *Physics of Semiconductor Devices*, 3rd ed.; John Wiley & Sons: Hoboken, NJ, 2006.
(61) Cooper, J. K.; Gul, S.; Toma, F. M.; Chen, L.; Liu, Y. S.; Guo, J.; Ager, J. W.; Yano, J.; Sharp, I. D. Indirect Bandgap and Optical Properties of Monoclinic Bismuth Vanadate. *J. Phys. Chem. C* **2015**, *119*, 2969−2974.

DOI: 10.1021/jacs.9b07295
J. Am. Chem. Soc. 2019, 141, 15932−15941